

# Error mitigated quantum computational chemistry

Sam McArdle,<sup>1,\*</sup> Xiao Yuan,<sup>1</sup> and Simon Benjamin<sup>1,†</sup>

<sup>1</sup>*Department of Materials, University of Oxford, Parks Road, Oxford OX1 3PH, United Kingdom*  
(Dated: December 14, 2024)

Variational algorithms may solve important chemistry problems on near-future quantum computers. However, their potential is limited by hardware errors. It is therefore crucial to develop ways to mitigate these errors, with minimal additional resources. Here, we propose a stabiliser-based modification to the variational quantum eigensolver which enables the detection of around 66 % of depolarising errors. We use a single additional qubit to check conserved molecular quantities. Numerical simulations show that our method is able to significantly increase the accuracy of noisy chemistry calculations, especially when combined with other error mitigation techniques.

Unlike their classical counterparts, quantum computers can efficiently simulate large quantum systems [1–3]. Classically, we are unable to exactly model systems larger than a few atoms [4]. In contrast, we can efficiently find the ground states of systems such as the Hubbard model or molecules using a quantum computer [5]. Accurately determining the electronic structure of molecules enables us to predict reaction rates [6] - a first step towards developing new materials [7], better catalysts [8] and more effective medicines [9].

On first inspection, transformative chemistry simulations seem tantalisingly close, requiring only around 100 logical qubits [8]. This is not much larger than current quantum devices, which have on the order of ten physical qubits. However, it is necessary to determine the required error correction overhead needed to convert these physical qubits into suitably protected logical qubits. This is determined by the error rates and required number of gates. Previous works have shown that the number of gates required is on the order of  $10^6 - 10^9$  [10–12], which would necessitate around two billion physical qubits [8]. While recent work has reduced requirements to around one million physical qubits [13], this remains many years beyond our current capabilities.

This narrative was altered by the arrival of variational quantum algorithms for solving chemistry problems [14–16], most notably the variational quantum eigensolver (VQE). These hybrid algorithms replace the long gate sequence required by phase estimation for a polynomial number of short circuits. After each circuit, the qubits are measured and reinitialised. This dramatically reduces the coherence time required, and has led to the suggestion that these variational algorithms may not require error correction [17]. Indeed, previous small experimental demonstrations of the VQE have shown it to be resilient to systematic errors, and better suited to near-term hardware than phase estimation [18]. However, larger experimental demonstrations have shown

that noise can dramatically corrupt results [19, 20]. This is perhaps unsurprising; depending on the method used to map the chemistry problem onto a quantum computer, errors can add or remove electrons, changing the molecule being simulated. Moreover, errors increase the variance of the energy measurements obtained from the VQE, increasing the number of measurements needed to obtain a precise result [21].

To date, several methods for mitigating errors in near-term quantum hardware have been proposed: the linear [22, 23] and exponential [24] extrapolation methods, the quasi-probability method [23, 24] and the quantum subspace expansion (QSE) [25]. The linear extrapolation method and QSE have recently been experimentally demonstrated [26, 27], and were successful in accurately finding the ground states of small molecules in the presence of noise. However, these schemes have various limitations. The linear extrapolation method is limited to circuits where the expected number of errors is much less than one. The exponential extrapolation and quasi-probability methods can work when the expected number of errors is approximately one, but require longer circuits with lower error rates than is currently possible [24]. Moreover, the quasi-probability technique is more difficult to implement experimentally, requiring gate set tomography. The QSE may require a large number of additional measurements, thus increasing the time cost of the algorithm.

Motivated by these limitations, we have developed a new scheme for mitigating errors in near-term quantum chemistry calculations. Our method uses stabiliser checks on a suitably constructed variational trial state to detect errors. While requiring minimal additional resources, it dramatically improves the accuracy of variational quantum chemistry calculations. Our scheme is even more effective in combination with the extrapolation method, and could also be combined with the QSE. In the following section, we introduce the stabiliser-VQE method, and provide analytical motivation for its effectiveness. We then numerically demonstrate our technique by using it to detect errors in an electronic structure calculation on the hydrogen molecule.

---

\* samuel.mcardle@materials.ox.ac.uk

† simon.benjamin@materials.ox.ac.uk

## I. ERROR DETECTING VQE

### A. Conventional VQE

We can use the VQE to find the ground state energy of molecular Hamiltonians. Further background on computational chemistry can be found in Appendix A, but we briefly outline the essential elements here. We seek to arrange electrons among spin-orbitals such that the energy of the molecule is minimised. We must map the molecular fermionic operators to qubit operators, which we do using the Jordan-Wigner (JW) transform, as the alternative Bravyi-Kitaev mapping is more susceptible to errors than JW mapped states [21]. Under the JW mapping, each qubit represents a spin-orbital. We store the occupation number of an orbital in the  $|0\rangle$  or  $|1\rangle$  state of the qubit (unoccupied or occupied, respectively). The Hamiltonian produced by the JW mapping can be written as a linear combination of products of Pauli operators,

$$H = \sum_j^M g_j h_j = \sum_j^M g_j \prod_i \sigma_i^j, \quad (1)$$

where  $g_j$  are coefficients,  $\sigma_i^j$  represents one of  $I$ ,  $X$ ,  $Y$ , or  $Z$ ,  $i$  denotes which qubit the operator acts on, and  $j$  denotes which term in the Hamiltonian we apply. An example of a typical Pauli string in the Hamiltonian is,

$$h_j = X_0 Y_1 Y_2 X_3 Z_4 Z_5. \quad (2)$$

The VQE, as proposed in Ref. [14], augments a small quantum processor with a powerful classical computer. The quantum computer is used for classically intractable state preparation, and measurement of the energy of the state. The state preparation circuit consists of a number of parametrised gates. The circuit used is known as the ansatz, denoted by  $U(\vec{\theta})$ . This circuit produces a trial state,  $|\psi(\vec{\theta})\rangle$ . The values of the parameters and the energy expectation value of the state they create are input into a classical optimisation algorithm. This algorithm outputs new circuit parameters, which are intended to produce a state that is lower in energy. By repeating this process, and invoking the Ritz-Rayleigh variational principle [28], we are able to converge to the ground state of the system, if local minima can be avoided [17, 29].

The energy of the state is not measured in one go, but is calculated by summing the expectation values of each term in the Hamiltonian. To obtain each expectation value, we must repeatedly perform the circuit, measure the state produced, and reinitialise, as shown in Fig. 1.

### B. Stabiliser-VQE

In variational chemistry calculations, it is beneficial to initialise the register in the Hartree-Fock (mean-field)

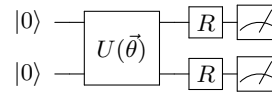


FIG. 1. A VQE circuit for a single measurement of a Hamiltonian term.  $U(\vec{\theta})$  applies the ansatz such that  $|\psi\rangle = |\psi(\vec{\theta})\rangle = U(\vec{\theta})|0\rangle$ . The  $R$  gates rotate the basis to measure  $h_j$ . For example, if  $h_j = X_0 X_1$  then  $R_0$  and  $R_1$  are Hadamard gates. Measurement is in the computational basis.

state, and use a particle-number and spin conserving ansatz [30, 31]. This produces states with the correct number of: electrons,  $N_e$ , spin-up electrons,  $N_\uparrow$ , and spin-down electrons,  $N_\downarrow$ . We refer to these states as ‘physical’ states. These physical states are eigenvectors of the electron number, spin-up number, and spin-down number operators. As these quantities are conserved, their relevant parity operators are also conserved;  $\hat{P}_N |\psi\rangle = P_N |\psi\rangle = (-1)^N |\psi\rangle$  and  $\hat{P}_{N_\uparrow/\downarrow} |\psi\rangle = P_{N_\uparrow/\downarrow} |\psi\rangle = (-1)^{N_\uparrow/\downarrow} |\psi\rangle$ . In analogy with error correcting codes, the states generated by the ansatz are said to be stabilised by these three parity operators.

There are some ansätze, such as those suggested in Refs. [31, 32] which are constructed from individual gates which conserve particle number and spin. If a single bit-flip error occurs, it will create or destroy an electron in one of the spin-orbitals, radically changing the state. For other number and spin conserving ansätze, like the unitary coupled cluster ansatz (which is constructed from individual gates which do not necessarily conserve particle number), a single error can propagate and degrade the final state even further. This can be catastrophic for the simulation results. A key concern for the VQE is preserving particle number, as states with electron number far from the true value appear to have a larger energy variance than those with smaller particle number errors [21]. We present below a method of detecting and removing some of these damaging errors, while still retaining the low qubit resources and gate count of the VQE.

In order to detect errors, we introduce an ancilla qubit, and use it to perform measurements of the conserved quantities. We will discuss three such measurements below. When deriving error detection rates for these three checks, we make the following assumptions:

1. The errors are symmetric and depolarising.
2. The error rate is low, such that only one gate malfunctions in the circuit.
3. The ansatz circuit is built from individual gates which conserve particle number and spin.
4. Single qubit gate errors are negligible compared to two qubit gate errors.

While our method is still applicable under higher noise rates, different noise models, and using other number

conserving ansatz (such as the unitary coupled cluster ansatz), an analytic bound on the error detection rate becomes much more difficult.

The most simple stabiliser measurement checks the total electron number parity. This procedure is shown in Fig. 2, and enables the detection of any error which changes the electron number parity by one. Under the assumptions described above, we are able to detect and remove 53 % of error events (we can detect the 8/15 errors in the depolarising noise model which change the electron number parity, as described in Appendix B). Filtering errors in this way dramatically increases the signal-to-noise ratio of our expectation value, improving its accuracy and reducing the variance (and hence the total number of measurements needed).

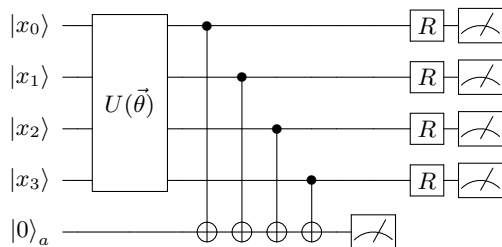


FIG. 2. The stabiliser-VQE circuit to check the electron number parity of a trial state, which should have the correct number of electrons. The ancilla should be measured in the state  $|\frac{1}{2}(1 - (-1)^{N_e})\rangle$ . If errors occur, and the measured value of the ancilla is not correct, the measurements on the main qubit register are not performed, and the circuit is reinitialised. The qubits are initialised in  $x_i = 0$  or 1 such that the register is in the Hartree-Fock state of the molecule.

We can perform measurements of the other conserved quantities to detect an even greater number of errors. We can perform the circuit shown in Fig. 3 to measure both the spin-up parity and spin-down parity. This enables us to detect certain combinations of two qubit errors, as well as the errors detectable using the total electron number parity check. Under the assumptions listed above, the proportion of two qubit bit-flip errors we can detect tends to 1/2 from above as the number of spin orbitals increases (shown in Appendix B). This means we can effectively filter out 66 % of errors (10/15 two qubit gate errors in the depolarising noise model).

We can also measure the electron number and spin numbers directly. This enables the detection of errors which change the electron number or spin of the state, even if they do not change the electron number parity or spin parities. The circuit in Fig. 4 measures the electron number, and only requires a single ancilla qubit. It can be verified that the circuit produces the state

$$|\phi\rangle = \frac{1}{\sqrt{2}}(|0_a\rangle + e^{N_e \pi i / 2^{m-1}} |1_a\rangle) |\psi\rangle \quad (3)$$

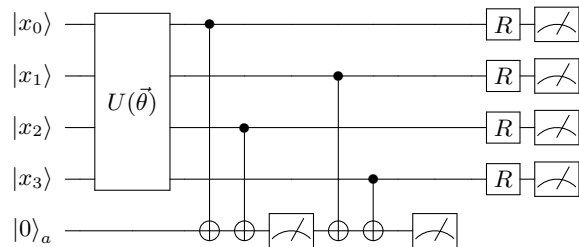


FIG. 3. A circuit to measure both the spin-up parity and spin-down parity. We first compute the spin-up parity onto the ancilla, and measure it. We then reinitialise the ancilla in  $|0\rangle$ , and measure the spin-down parity.

where  $|\psi\rangle$  is the state of the register qubits, and  $m$  is the number of bits needed to write  $N_e$  in binary. As we know the ancilla state that is produced in the absence of errors *a priori*, we can verify that  $|\psi\rangle$  describes a state with the correct number of electrons by projecting the ancilla onto the state in Eq. (3).

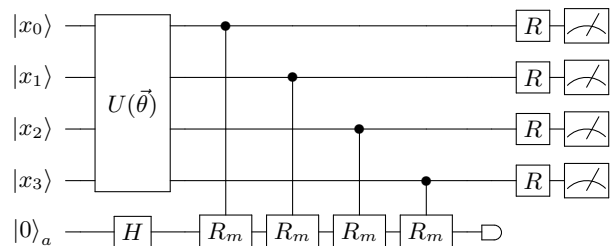


FIG. 4. The circuit which measures the electron number,  $N_e$ . The  $R_m$  gates are given by  $\text{diag}(1, e^{2\pi i / 2^m})$  where  $m$  is the number of bits needed to represent  $N_e$  in binary. The ancilla is measured by projecting it onto the state in Eq. (3).

We can measure the spin-up and spin-down numbers using a similar procedure. Using these additional pieces of information, we can increase the proportion of errors detected. The exact fraction of errors that can be detected will depend on the trial state produced by the ansatz. We note that it may be difficult to realise the controlled- $R_m$  gate experimentally. As a consequence, the double parity check discussed above is likely more practical for near-future chemistry calculations.

We have found that it is also possible to use a different circuit variant to detect errors in the VQE. This circuit is described in Appendix C. The advantage of this alternative circuit is that we only need to measure a single ancilla qubit to determine the expectation value of the Hamiltonian term  $h_j$ . This enables us to reduce the impact of qubit readout errors on our result. However, this circuit is only able to detect an electron number parity error, and so is not as useful for mitigating gate errors as the methods described above.

Using an ansatz which conserves particle number and spin produces a state that is a general superposition of all vectors with suitable occupation values. For example, for the most simple model of the hydrogen molecule, this state can be written as (see Appendix D)

$$|\psi^{H_2}\rangle = \alpha|0011\rangle + \beta|1100\rangle + \gamma|1001\rangle + \delta|0110\rangle. \quad (4)$$

It is not possible to detect phase errors in such a state, which provides a limit to the effectiveness of our method. As a result, improving the error resilience of our method will require additional tools. We discuss this further in Sec. III.

As we are not able to detect all errors, the results will not be noise free. Consequently, we can combine the stabiliser-VQE technique with other methods of error mitigation to further improve accuracy. The most simple approach is to use the detection method to filter out errors, and then use the extrapolation technique to obtain highly accurate results.

## II. NUMERICAL SIMULATIONS

In this section we test our method’s efficacy at reducing the impact of errors in a VQE calculation. We consider the most simple model of molecular hydrogen ( $H_2$ ), which consists of two electrons distributed in four spin orbitals. We used a spin-conserving unitary coupled cluster (UCC) ansatz applied to the Hartree-Fock state for  $H_2$ . Following the procedure of Ref. [21], we did not consider the parameter update step of the VQE, which enabled us to examine our results without consideration of a classical optimisation algorithm. Instead, we sought the effect of errors on energy measurements. More information about  $H_2$ , and the circuit diagram for the UCC ansatz used, are given in Appendix D. Numerical simulations were performed using the Quantum Exact Simulation Toolkit (QuEST) [33].

We used a symmetric depolarising noise model in all calculations, and assumed that the two qubit error rate was 10 times larger than the single qubit error rate. To detect errors, we performed checks of both the spin-up and spin-down parity numbers, using the circuit shown in Fig. 3. When performing the error detection procedure, we discarded results for which the measured parities were not equal to the true parities. We designed our simulations to mimic the actions of an experimentalist; the expectation value of each term in the Hamiltonian was found by repeating the circuit and measurement procedure many times. We used  $10^6$  samples for each expectation value in order to reduce the shot noise in our results to within ‘chemical accuracy’ (1.6 mHartree). We used the same total number of samples for extrapolation, which were divided equally between two points for a linear extrapolation. The first point was taken with the target error rate, while the second point was taken with the error rate doubled.

Initially, we considered energy measurements on a trial state that contained all four possible vectors, as described by Eq. (4). Our calculations were performed at an inter-nuclear separation of 0.75 Å. We measured the energy of the state constructed by the ansatz under the following conditions:

1. No parity check, No errors, No extrapolation.
2. No parity check, Errors, No extrapolation.
3. No parity check, Errors, Extrapolation.
4. Parity check, Errors, No extrapolation.
5. Parity check, Errors, Extrapolation.

We compare these results to the true energy extracted in the limit of infinite measurements and no gate errors. The first test quantifies the shot noise in our results. The second simulation shows the impact of gate errors, which is the result that would be obtained from a standard VQE calculation with these noise rates. The results are shown in Fig. 5, using two qubit gate error rates ranging from 0.5 % to 7 %. There were 21 single qubit gates and 22 two qubit gates in the UCC ansatz circuit - which we approximated as 24 two qubit gates when calculating the expected number of errors in the circuit. The parity checks contributed an additional 8 two qubit gates, but were not included in the expected number of errors estimate.

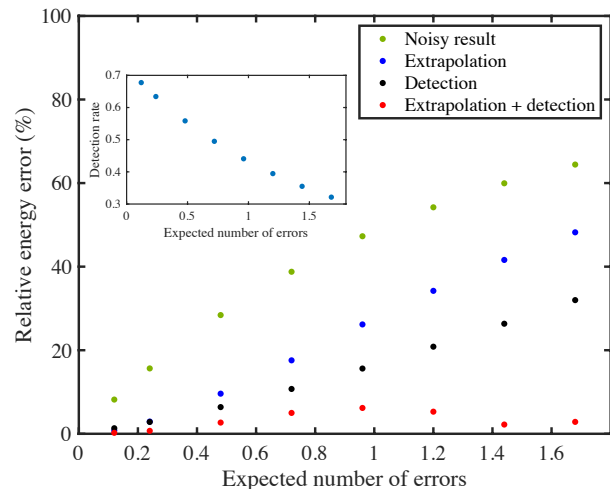


FIG. 5. Comparing methods of mitigating errors in variational chemistry simulations of  $H_2$ . The detection rate was obtained numerically. Shot noise in the absence of gate errors was 0.1 mHartree. The true energy value was -1.1227 Hartree.

We see from Fig. 5 that the error detection method alone dramatically improves the accuracy of our energy measurements. At high error rates, the detection method is much more effective than linear extrapolation, while when the expected number of errors is less than around 0.3, the two methods become equally effective. We observe from the inset plot that the fraction of detected errors falls approximately linearly with increasing error

rate. When the error rate is small we detect around 66 % of errors, as predicted in the previous section. At higher error rates, multiple errors are able to occur in the circuit, which reduces the fraction of errors that we can detect. The greatest benefit is obtained by combining the extrapolation and detection methods, which consistently yields results that are far more accurate than either method yields in isolation. Moreover, the accuracy obtained does not worsen significantly as the error rate increases, unlike the detection and extrapolation methods on their own.

We also used our method to reduce errors when calculating the dissociation curve of  $H_2$ . For these calculations, we used the values of the parameters which give the ground state of  $H_2$  at the corresponding internuclear separation. We compare the true energy values with: noisy measurements without error mitigation, noisy measurements with extrapolation, and noisy measurements with detection and extrapolation. The two qubit gate error rate was  $5 \times 10^{-3}$ , which has been achieved in a controlled setting, and should be targetable in near-future quantum computers [34–36]. We note that while previous experimental VQE calculations of  $H_2$  have achieved good levels of accuracy with higher error rates [18–20, 26, 27], these experiments used circuits with fewer gates (and often fewer qubits) than the simulations presented in Fig. 6.

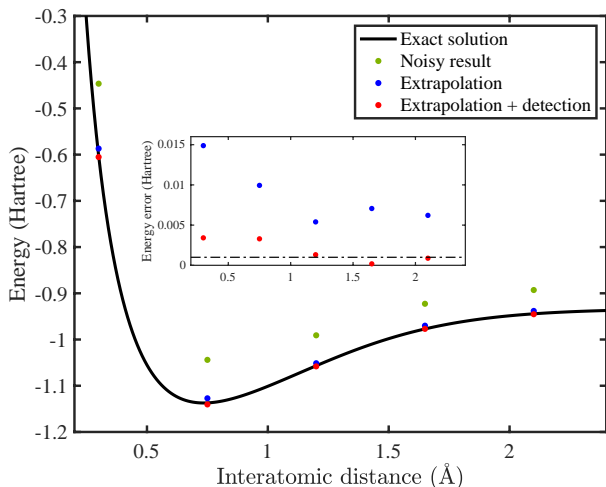


FIG. 6. Comparing methods of mitigating errors in variational chemistry simulations of  $H_2$ . The 2 qubit gate error is  $5 \times 10^{-3}$ . The green points are without error mitigation, blue points with extrapolation, and red points with extrapolation and detection. The inset plot shows the residual from the true value for both mitigation methods. The dashed line in the inset plot marks chemical accuracy (1.6 mHartree).

We see from Fig. 6 that energy measurements are dramatically improved by using the combination of error detection and extrapolation. Combining error detection with extrapolation is once again more effective than using extrapolation alone. The inset plot shows

that our method can obtain chemically accurate energies, even when the results would otherwise be completely corrupted by noise. In the most extreme case, the deviation from the true value is reduced by a factor of 40 by using detection and extrapolation, when compared to the unmitigated result. On average, we were able to detect 64.9 % of the errors which occurred during the circuit, close to the analytic upper bound derived in Appendix B. This suggests that our error mitigation technique can benefit near-future quantum computational chemistry calculations, especially when used in conjunction with previously developed methods.

### III. DISCUSSION

In this work, we have introduced a method to mitigate errors in near-term quantum computational chemistry calculations. The procedure involves using parity checks to detect errors. When using suitably constructed ansätze, around 66 % of errors can be detected. Our method requires minimal additional resources, needing only one ancilla qubit and  $N$  controlled-NOT gates (where  $N$  is the number of register qubits). We can extend the method to detect changes in the electron and spin number of trial states, which gives a higher detection rate.

Our method dramatically improves accuracy in variational quantum eigensolver calculations, especially when combined with the extrapolation method of error mitigation. We simulated a VQE calculation of the hydrogen molecule, and found that the deviation from the true result is reduced by more than an order of magnitude using our technique. As our method can be easily implemented, it can immediately benefit quantum computational chemistry calculations.

While our method can detect a large proportion of errors, additional mechanisms will be required to provide suitable error resilience for long circuits on non-error corrected machines. We highlight two possible avenues towards this goal. Our method may be able to be combined with a two qubit phase-error detection code. However, constructing a gate set that does not turn physical qubit errors into logical qubit errors requires additional consideration. Alternatively, one could design new ansätze which conserve quantities beyond particle number and spin. It was noted in Ref. [37] that the Hamiltonians of small molecules contain several symmetries. If ansätze could be designed which respect these symmetries, additional stabiliser checks would be available to detect and filter an even greater number of errors.

**Acknowledgements.** We thank S. Endo for insightful discussions. This work was supported by BP plc and the EPSRC National Quantum Technology Hub in Networked Quantum Information Technology (EP/M013243/1). We acknowledge the use of the University of Oxford Advanced Research Computing facility.

- [1] P. Dirac, Proceedings of the Royal Society of London **123** (1929), 10.1098/rspa.1929.0094.
- [2] R. P. Feynman, International Journal of Theoretical Physics **21**, 467 (1982).
- [3] S. Lloyd, Science **273**, 1073 (1996), <http://science.sciencemag.org/content/273/5278/1073.full.pdf>.
- [4] I. Kassal, S. P. Jordan, P. J. Love, M. Mohseni, and A. Aspuru-Guzik, Proceedings of the National Academy of Sciences **105**, 18681 (2008).
- [5] A. Aspuru-Guzik, A. D. Dutoi, P. J. Love, and M. Head-Gordon, Science **309**, 1704 (2005).
- [6] J. Romero, R. Babbush, J. R. McClean, C. Hempel, P. Love, and A. Aspuru-Guzik, arXiv preprint arXiv:1701.02691 (2017).
- [7] R. Babbush, N. Wiebe, J. McClean, J. McClain, H. Neven, and G. K.-L. Chan, Phys. Rev. X **8**, 011044 (2018).
- [8] M. Reiher, N. Wiebe, K. M. Svore, D. Wecker, and M. Troyer, Proceedings of the National Academy of Sciences (2017), 10.1073/pnas.1619152114.
- [9] A. Aspuru-Guzik, R. Lindh, and M. Reiher, ACS Central Science **4**, 144 (2018), <https://doi.org/10.1021/acscentsci.7b00550>.
- [10] D. Wecker, B. Bauer, B. K. Clark, M. B. Hastings, and M. Troyer, Phys. Rev. A **90**, 022305 (2014).
- [11] M. B. Hastings, D. Wecker, B. Bauer, and M. Troyer, QIC **15** (2015).
- [12] D. Poulin, M. B. Hastings, D. Wecker, N. Wiebe, A. C. Doherty, and M. Troyer, QIC **15** (2015).
- [13] R. Babbush, C. Gidney, D. W. Berry, N. Wiebe, J. McClean, A. Paler, A. Fowler, and H. Neven, arXiv preprint arXiv:1805.03662 (2018).
- [14] A. Peruzzo, J. McClean, P. Shadbolt, M.-H. Yung, X.-Q. Zhou, P. J. Love, A. Aspuru-Guzik, and J. L. O'Brien, Nature communications **5** (2014).
- [15] M.-H. Yung, J. Casanova, A. Mezzacapo, J. McClean, L. Lamata, A. Aspuru-Guzik, and E. Solano, Scientific reports **4**, 3589 (2014).
- [16] J. R. McClean, J. Romero, R. Babbush, and A. Aspuru-Guzik, New Journal of Physics **18**, 023023 (2016).
- [17] D. Wecker, M. B. Hastings, and M. Troyer, Phys. Rev. A **92**, 042303 (2015).
- [18] P. J. J. O'Malley, R. Babbush, I. D. Kivlichan, J. Romero, J. R. McClean, R. Barends, J. Kelly, P. Roushan, A. Tranter, N. Ding, B. Campbell, Y. Chen, Z. Chen, B. Chiaro, A. Dunsworth, A. G. Fowler, E. Jeffrey, E. Lucero, A. Megrant, J. Y. Mutus, M. Neeley, C. Neill, C. Quintana, D. Sank, A. Vainsencher, J. Wenner, T. C. White, P. V. Coveney, P. J. Love, H. Neven, A. Aspuru-Guzik, and J. M. Martinis, Phys. Rev. X **6**, 031007 (2016).
- [19] A. Kandala, A. Mezzacapo, K. Temme, M. Takita, M. Brink, J. M. Chow, and J. M. Gambetta, Nature **549**, 242 (2017).
- [20] C. Hempel, C. Maier, J. Romero, J. McClean, T. Monz, H. Shen, P. Jurcevic, B. Lanyon, P. Love, R. Babbush, A. Aspuru-Guzik, R. Blatt, and C. Roos, ArXiv e-prints (2018), arXiv:1803.10238 [quant-ph].
- [21] N. P. D. Sawaya, M. Smelyanskiy, J. R. McClean, and A. Aspuru-Guzik, Journal of Chemical Theory and Computation **12**, 3097 (2016), PMID: 27254482, <https://doi.org/10.1021/acs.jctc.6b00220>.
- [22] Y. Li and S. C. Benjamin, Phys. Rev. X **7**, 021050 (2017).
- [23] K. Temme, S. Bravyi, and J. M. Gambetta, Phys. Rev. Lett. **119**, 180509 (2017).
- [24] S. Endo, S. C. Benjamin, and Y. Li, arXiv preprint arXiv:1712.09271 (2017).
- [25] J. R. McClean, M. E. Kimchi-Schwartz, J. Carter, and W. A. de Jong, Phys. Rev. A **95**, 042308 (2017).
- [26] A. Kandala, K. Temme, A. D. Corcoles, A. Mezzacapo, J. M. Chow, and J. M. Gambetta, arXiv:1805.04492 (2018).
- [27] J. I. Colless, V. V. Ramasesh, D. Dahlen, M. S. Blok, M. E. Kimchi-Schwartz, J. R. McClean, J. Carter, W. A. de Jong, and I. Siddiqi, Phys. Rev. X **8**, 011021 (2018).
- [28] J. J. Sakurai and J. Napolitano, *Modern quantum mechanics* (Cambridge University Press, 2017).
- [29] S. McArdle, S. Endo, Y. Li, S. Benjamin, and X. Yuan, arXiv preprint arXiv:1804.03023 (2018).
- [30] J. R. McClean, S. Boixo, V. N. Smelyanskiy, R. Babbush, and H. Neven, arXiv preprint arXiv:1803.11173 (2018).
- [31] P. K. Barkoutsos, J. F. Gonthier, I. Sokolov, N. Moll, G. Salis, A. Fuhrer, M. Ganzhorn, D. J. Egger, M. Troyer, A. Mezzacapo, S. Filipp, and I. Tavernelli, ArXiv e-prints (2018), arXiv:1805.04340 [quant-ph].
- [32] I. D. Kivlichan, J. McClean, N. Wiebe, C. Gidney, A. Aspuru-Guzik, G. K.-L. Chan, and R. Babbush, Phys. Rev. Lett. **120**, 110501 (2018).
- [33] T. Jones, A. Brown, I. Bush, and S. Benjamin, (2018), arXiv:1802.08032.
- [34] R. Barends, J. Kelly, A. Megrant, A. Veitia, D. Sank, E. Jeffrey, T. C. White, J. Mutus, A. G. Fowler, B. Campbell, *et al.*, Nature **508**, 500 (2014).
- [35] C. J. Ballance, T. P. Harty, N. M. Linke, M. A. Sepiol, and D. M. Lucas, Phys. Rev. Lett. **117**, 060504 (2016).
- [36] T. Harty, D. Allcock, C. J. Ballance, L. Guidoni, H. Janacek, N. Linke, D. Stacey, and D. Lucas, Physical review letters **113**, 220501 (2014).
- [37] S. Bravyi, J. M. Gambetta, A. Mezzacapo, and K. Temme, arXiv preprint arXiv:1701.08213 (2017).
- [38] J. T. Seeley, M. J. Richard, and P. J. Love, The Journal of Chemical Physics **137**, 224109 (2012), <https://doi.org/10.1063/1.4768229>.
- [39] A. K. Ekert, C. M. Alves, D. K. L. Oi, M. Horodecki, P. Horodecki, and L. C. Kwak, Phys. Rev. Lett. **88**, 217901 (2002).
- [40] A. Y. Kitaev, Preprint at <http://arxiv.org/abs/quant-ph/9511026> (1995).
- [41] J. D. Whitfield, J. Biamonte, and A. Aspuru-Guzik, Molecular Physics **109**, 735 (2011), <https://doi.org/10.1080/00268976.2011.552441>.

## Appendix A: Computational chemistry

We can use the VQE to find the ground state energy of a molecular Hamiltonian. Following most of the previous work on near-term quantum computational chemistry, we use the second quantised formalism. We project the Hamiltonian onto a finite number of basis wavefunctions,  $\{\phi_p\}$ , which approximate spin-orbitals. Electrons are excited into, or de-excited out of, these orbitals by fermionic creation ( $a_p^\dagger$ ) or annihilation ( $a_p$ ) operators, respectively. These operators obey fermionic anti-commutation relations, which enforce the antisymmetry of the wavefunction, a consequence of the Pauli exclusion principle. In the second quantised representation, the electronic Hamiltonian is written as

$$H = \sum_{p,q} h_{pq} a_p^\dagger a_q + \frac{1}{2} \sum_{p,q,r,s} h_{pqrs} a_p^\dagger a_q^\dagger a_r a_s, \quad (\text{A1})$$

with

$$\begin{aligned} h_{pq} &= \int d\mathbf{x} \phi_p^*(\mathbf{x}) \left( \frac{\nabla_i^2}{2} - \sum_I \frac{Z_I}{|\mathbf{r} - \mathbf{R}_I|} \right) \phi_q(\mathbf{x}), \\ h_{pqrs} &= \int d\mathbf{x}_1 d\mathbf{x}_2 \frac{\phi_p^*(\mathbf{x}_1) \phi_q^*(\mathbf{x}_2) \phi_s(\mathbf{x}_1) \phi_r(\mathbf{x}_2)}{|\mathbf{r}_1 - \mathbf{r}_2|}, \end{aligned} \quad (\text{A2})$$

where  $\mathbf{x}$  is a spatial and spin coordinate.

This fermionic Hamiltonian can be mapped to a qubit Hamiltonian by employing an encoding method. The two most common methods are the Jordan-Wigner (JW) and Bravyi-Kitaev (BK) mappings. In this work, we use the JW encoding, as it was found in Ref. [21] that the BK mapping was more susceptible to errors than JW mapped states. In the JW encoding, we store the occupation number of an orbital in the  $|0\rangle$  or  $|1\rangle$  state of a qubit (unoccupied or occupied, respectively). The mapping between the fermionic creation and annihilation operators and qubit gates is given by [38]

$$\begin{aligned} a_p &= (X_p + iY_p) \otimes Z_{p-1} \otimes \cdots \otimes Z_0, \\ a_p^\dagger &= (X_p - iY_p) \otimes Z_{p-1} \otimes \cdots \otimes Z_0. \end{aligned} \quad (\text{A3})$$

The  $X$  and  $Y$  operators change the occupation number of the target orbital, while the string of  $Z$  operators enforce electron exchange antisymmetry. The JW mapped Hamiltonian of a molecule can be written as a linear combination of products of Pauli operators,

$$H = \sum_j^M g_j h_j = \sum_j^M g_j \prod_i \sigma_i^j, \quad (\text{A4})$$

where  $g_j$  are coefficients,  $\sigma_i^j$  represents one of  $I$ ,  $X$ ,  $Y$ , or  $Z$ ,  $i$  denotes which qubit the operator acts on, and  $j$  denotes which term in the Hamiltonian we apply. For example,

$$h_j = X_0 Y_1 Y_2 X_3 Z_4 Z_5. \quad (\text{A5})$$

As each term in the fermionic Hamiltonian contains an even number of creation and annihilation operators, each term in the qubit Hamiltonian will contain an even number of  $X$  or  $Y$  operators, and thus will conserve particle number parity.

## Appendix B: Error detection rates

When deriving error detection rates, we make the following assumptions:

1. The errors are symmetric and depolarising.
2. The error rate is low, such that only one gate malfunctions in the circuit.
3. The ansatz circuit is built from individual gates which conserve particle number and spin [31, 32].
4. Single qubit gate errors are negligible compared to two qubit gate errors.

While our method is still applicable under higher noise rates, different noise models, and using other number conserving ansätze (such as the unitary coupled cluster ansatz), an analytic bound on the error detection rate becomes much more difficult.

## 1. Total electron number parity check

By performing a single parity check of the total electron number, we are able to detect 53 % of errors under the above assumptions. In the symmetric depolarising noise model the following errors are equally likely following a two qubit gate between qubits  $i$  and  $j$ :

$$\begin{aligned} X_i I_j, I_i X_j, Y_i I_j, I_i Y_j, X_i Z_j, Z_i X_j, Y_i Z_j, Z_i Y_j, \\ Z_i I_j, I_i Z_j, X_i X_j, Y_i Y_j, Z_i Z_j, X_i Y_j, Y_i X_j. \end{aligned} \quad (\text{B1})$$

We can see that all of the errors in the top row change the electron number parity of a state vector. As a result, using a single parity check, we can detect  $8/15 \approx 53\%$  of these errors.

This is true both if the error occurs during the ansatz circuit (we can detect  $X_i I_j, I_i X_j, Y_i I_j, I_i Y_j, X_i Z_j, Z_i X_j, Y_i Z_j, Z_i Y_j$  out of the 15 possible errors on two of the register qubits) or during the parity check gate sequence (we can detect  $X_r X_a, X_r Y_a, Y_r X_a, Y_r Y_a, Z_r X_a, Z_r Y_a, I_r X_a, I_r Y_a$ , where  $r$  and  $a$  denote register and ancilla qubits, respectively).

## 2. Spin-up and spin-down parity check

Using the spin-up and spin-down parity checks, we can detect additional errors beyond the 8/15 detectable using the electron number parity measurement. We will be able to detect certain two qubit errors, which change the value of either spin-parity. However, we will not be able to detect all two qubit bit-flip errors.

There are  $\binom{M}{2} = \frac{M(M-1)}{2}$  ways of distributing a two qubit bit-flip error between the  $M$  spin-orbitals. We are unable to detect errors which both occur on the spin-up orbitals, or both on spin-down orbitals. We are able to detect errors which occur on one orbital of each spin. There are  $\binom{M/2}{1} = M/2$  ways of distributing an error amongst half of the orbitals. As a result, there are  $\frac{M^2}{4}$  errors we can detect.

For a 2 spin orbital system, we can detect  $\frac{2^2/4}{(2 \times 1)/2} = 100\%$  of double bit-flip errors. For a 4 spin orbital system, this reduces to 66 % of double bit-flip errors.

When  $M$  is large, we can detect  $\frac{M^2/4}{M(M-1)/2} \approx \frac{M^2/4}{M^2/2} = \frac{1}{2}$  of double bit-flip errors. As there are four possible types of double bit-flip errors, and we can detect half of the occurrences of each of them, this effectively increases the number of error events we can detect by 2/15, to 10/15  $\approx 66\%$ .

## Appendix C: Alternative stabiliser-VQE circuit

Here we provide more detail on the alternative circuit mentioned in the main text, which can be used to reduce noise due to readout errors. We first show that the circuit given by Fig. 7 [39, 40] gives the desired outcome for the VQE;  $\langle \psi | h_j | \psi \rangle$ . Stepping through the circuit, we find that:

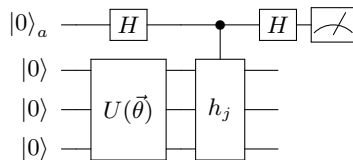


FIG. 7. The alternative method of performing a single measurement of term  $h_j$  in the Hamiltonian. The ansatz circuit  $U(\vec{\theta})$  creates a physical state;  $|\psi\rangle = |\psi(\vec{\theta})\rangle = U(\vec{\theta})|\bar{0}\rangle$ . The controlled- $h_j$  gate is easy to realise in practice, as  $h_j$  is a product of Pauli terms on different qubits, so it can be implemented as a sequence of controlled Pauli gates.

$$\begin{aligned}
|\bar{0}\rangle|0\rangle_a &\rightarrow \frac{1}{\sqrt{2}}(|\psi\rangle|0\rangle_a + |\psi\rangle|1\rangle_a) \\
&\rightarrow \frac{1}{\sqrt{2}}(|\psi\rangle|0\rangle_a + h_j|\psi\rangle|1\rangle_a) \\
&\rightarrow \frac{1}{2}[|0\rangle_a(|\psi\rangle + h_j|\psi\rangle) + |1\rangle_a(|\psi\rangle - h_j|\psi\rangle)] = |\phi\rangle
\end{aligned} \tag{C1}$$

Measuring the ancilla in the computational basis gives

$$\langle\phi|Z_a|\phi\rangle = \frac{1}{4}(2\langle\psi|\psi\rangle + 2\langle\psi|h_j|\psi\rangle) - \frac{1}{4}(2\langle\psi|\psi\rangle - 2\langle\psi|h_j|\psi\rangle) = \langle\psi|h_j|\psi\rangle, \tag{C2}$$

the same result as the conventional VQE circuit, as required. The circuit has obtained this result by performing a single measurement each time, thus reducing noise due to readout errors when compared to the normal direct measurement VQE protocol.

We can also use this circuit to extract parity information about the qubits ‘for free’. When the circuit and measurement are performed, the ancilla will either be measured in the  $|0\rangle_a$  or the  $|1\rangle_a$  state. The register is correspondingly in either

$$|0\rangle_a \rightarrow |\phi_R\rangle = \frac{|\psi\rangle + h_j|\psi\rangle}{\sqrt{2(1 + \langle\psi|h_j|\psi\rangle)}} \tag{C3}$$

$$|1\rangle_a \rightarrow |\phi_R\rangle = \frac{|\psi\rangle - h_j|\psi\rangle}{\sqrt{2(1 - \langle\psi|h_j|\psi\rangle)}} \tag{C4}$$

which we write as  $|\phi_R^\pm\rangle$ .

In the Jordan-Wigner encoding, the Pauli terms in the Hamiltonian,  $h_j$ , contain an even number of  $X$  and  $Y$  operators, and thus conserve electron number parity. Denoting the parity operator by  $\hat{P}$ , we find that  $\hat{P}|\psi\rangle = (-1)^{N_e}|\psi\rangle$  and  $\hat{P}h_j|\psi\rangle = (-1)^{N_e}h_j|\psi\rangle$ , where  $N_e$  is the number of electrons in the molecule. As a result, the register state is an eigenstate of the parity operator, and so we can measure this stabiliser quantity, as shown in Fig. 8. If a single bit-flip error has occurred, this will change the measured parity. If  $\langle\hat{P}\rangle \neq (-1)^{N_e}$ , we can discard the measurement result.

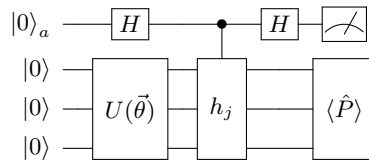


FIG. 8. We perform a parity measurement on the register after the ancilla has been measured in order to detect errors.

In the limit of small error rates, we consider that at most a single error happens. We assume here that no gate errors occur in the circuit, but a single readout error occurs. Using the circuit in Fig. 8, the probability that the error happens on the ancilla qubit is  $1/N$  where  $N$  is the total number of qubits. If the error occurs on the ancilla qubit, its value will be corrupted. In contrast, the parity measurement will yield the correct result. This means we will not filter the corrupted result, reducing the accuracy of our expectation value measurement. In the other  $(N - 1)/N$  cases, the readout error occurs on one of the register qubits. This causes us to incorrectly assert that the state  $|\psi\rangle$  is not a physical state, and therefore wrongly filter it out. However, our measured expectation value is not degraded much by this. When the number of qubits is large, the readout errors are much more likely to occur on the register qubits, and so we are still able to obtain an accurate expectation value.

In contrast, when considering the circuit shown in Fig. 2 in the main text, we find that the opposite is true. If only a single readout error occurs, it is much more likely to occur on the register qubits than on the ancilla. As a result, we are likely to accept a corrupted state, producing a less accurate expectation value. While this sounds like a significant disadvantage, we note that two qubit error rates are currently higher than readout error rates. Moreover,

the number of two qubit gates in the circuit will be much larger than the number of qubits. Therefore, it is much more likely that if only a single error occurs, it will occur in the circuit. Moreover, this circuit variant is only capable of checking the total electron parity, and not the spin up or down parities.

### Appendix D: UCC ansatz and the hydrogen molecule

When solving the electronic structure problem for the hydrogen molecule in a minimal basis, we construct four molecular orbitals,

$$\begin{aligned} |\sigma_{g\uparrow}\rangle &= \frac{1}{\sqrt{2}}(|1s_{A\uparrow}\rangle + |1s_{B\uparrow}\rangle), & |\sigma_{g\downarrow}\rangle &= \frac{1}{\sqrt{2}}(|1s_{A\downarrow}\rangle + |1s_{B\downarrow}\rangle), \\ |\sigma_{u\uparrow}\rangle &= \frac{1}{\sqrt{2}}(|1s_{A\uparrow}\rangle - |1s_{B\uparrow}\rangle), & |\sigma_{u\downarrow}\rangle &= \frac{1}{\sqrt{2}}(|1s_{A\downarrow}\rangle - |1s_{B\downarrow}\rangle), \end{aligned} \quad (\text{D1})$$

where  $A$  and  $B$  denote which of the two protons the  $1s$  orbital is centred on. We can write a Jordan-Wigner (JW) mapped state vector as

$$|\psi\rangle = |\sigma_{u\downarrow}\sigma_{u\uparrow}\sigma_{g\downarrow}\sigma_{g\uparrow}\rangle, \quad (\text{D2})$$

where each entry is 1 if the orbital is occupied, and 0 if it is vacant. Using the JW encoding, the 4 qubit Hamiltonian for  $\text{H}_2$ , given by [38]

$$\begin{aligned} H = & h_0I + h_1Z_0 + h_2Z_1 + h_3Z_2 + h_4Z_3 + h_5Z_0Z_1 + h_6Z_0Z_2 + h_7Z_1Z_2 + h_8Z_0Z_3 + \\ & h_9Z_1Z_3 + h_{10}Z_2Z_3 + h_{11}Y_0Y_1X_2X_3 + h_{12}X_0Y_1Y_2X_3 + h_{13}Y_0X_1X_2Y_3 + h_{14}X_0X_1Y_2Y_3. \end{aligned} \quad (\text{D3})$$

The HF state for  $\text{H}_2$  is given by

$$|\psi_{HF}^{H_2}\rangle = |0011\rangle. \quad (\text{D4})$$

The most general state for  $\text{H}_2$  (which respects conservation of spin) is given by

$$|\psi^{H_2}\rangle = \alpha|0011\rangle + \beta|1100\rangle + \gamma|1001\rangle + \delta|0110\rangle. \quad (\text{D5})$$

We can construct such a state using the unitary coupled cluster (UCC) ansatz, considering single and double excitations above the HF state (UCCSD). The UCCSD operator is given by

$$U = e^{(T_1 - T_1^\dagger) + (T_2 - T_2^\dagger)}, \quad (\text{D6})$$

where

$$\begin{aligned} T_1 &= \sum_{i \in \text{virt}, \alpha \in \text{occ}} t_{i\alpha} a_i^\dagger a_\alpha, \\ T_2 &= \sum_{i, j \in \text{virt}, \alpha, \beta \in \text{occ}} t_{ij\alpha\beta} a_i^\dagger a_j^\dagger a_\alpha a_\beta, \end{aligned} \quad (\text{D7})$$

and  $\text{occ}$  are occupied orbitals,  $\text{virt}$  are initially unoccupied orbitals in the HF state, and  $t_{i\alpha}$  and  $t_{ij\alpha\beta}$  are variational parameters to be optimised. For  $\text{H}_2$ , the UCCSD operator takes the form

$$U = e^{t_{02}(a_2^\dagger a_0 - a_0^\dagger a_2) + t_{13}(a_3^\dagger a_1 - a_1^\dagger a_3) + t_{0123}(a_3^\dagger a_2^\dagger a_1 a_0 - a_0^\dagger a_1^\dagger a_2 a_3)}. \quad (\text{D8})$$

Splitting this operator up using Trotterization (with a single Trotter step) and using the JW encoding, we find that

$$\begin{aligned} (a_2^\dagger a_0 - a_0^\dagger a_2) &= \frac{i}{2}(X_2 Z_1 Y_0 - Y_2 Z_1 X_0) \\ (a_3^\dagger a_1 - a_1^\dagger a_3) &= \frac{i}{2}(X_3 Z_2 Y_1 - Y_3 Z_2 X_1) \\ (a_3^\dagger a_2^\dagger a_1 a_0 - a_0^\dagger a_1^\dagger a_2 a_3) &= \\ & \frac{i}{8}(X_3 Y_2 X_1 X_0 + Y_3 X_2 X_1 X_0 + Y_3 Y_2 Y_1 X_0 + Y_3 Y_2 X_1 Y_0 - X_3 X_2 Y_1 X_0 - X_3 X_2 X_1 Y_0 - Y_3 X_2 Y_1 Y_0 - X_3 Y_2 Y_1 Y_0). \end{aligned} \quad (\text{D9})$$

We can simplify this operator, and apply it using the circuit shown in Fig 9 [41].

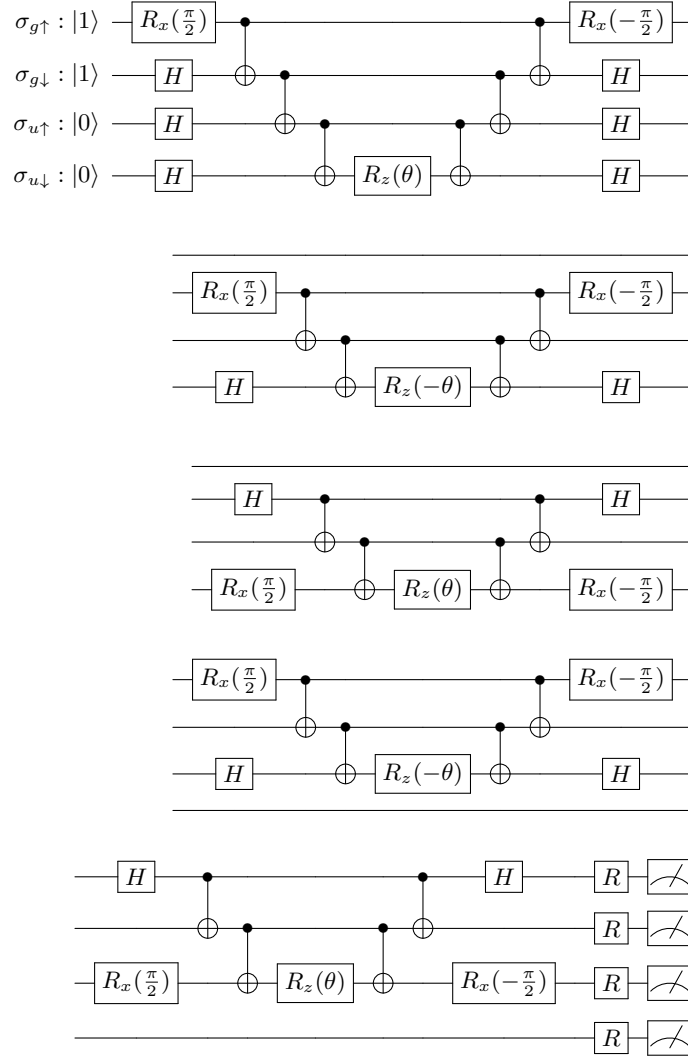


FIG. 9. The complete circuit used in our simulations to implement the UCCSD operator for  $H_2$ . The  $R_x(\frac{\pi}{2})$  and  $H$  gates rotate the basis such that the exponentiated operator applied to the corresponding qubit is either  $Y$  or  $X$ , respectively.